Mechanical failure of brittle thin films on polymers during bending by two-point rotation

Thin Solid Films 611 (2016) 107–116

Contents lists available at ScienceDirect

Thin Solid Films

journal homepage: www.elsevier.com/locate/tsf

Mechanical failure of brittle thin films on polymers during bending by two-point rotation

Qingling Guan [a,b], Jozua Laven [b], Piet C.P. Bouten [c,1], Gijsbertus de With [b,*]

[a] Materials innovation institute (M2i), Delft, The Netherlands
[b] Laboratory of Materials and Interface Chemistry, Eindhoven University of Technology, Den Dolech 2, 5600 MB Eindhoven, The Netherlands
[c] Philips Research Laboratories, High Tech Campus 4, 5656 AE Eindhoven, The Netherlands

ARTICLE INFO

Article history:
Received 2 October 2014
Received in revised form 6 April 2016
Accepted 16 May 2016
Available online 18 May 2016

Keywords:
Crack channeling
Thin-film barrier
Weibull statistics
Bent shape
Two-point rotation
Two-plate bending
Two-point bending
Internal strain
Barrier layer

ABSTRACT

The mechanical failure and internal strain when bending a brittle thin film on a flexible substrate was analyzed using an electro-mechanical method and optical microscopy. Bending was realized by clamping the ends of the sample and rotating the clamps in a two-point rotation (2PR) device, as elaborated in the paper. This test allows to impose both tensile and compressive strains on the brittle layer, in a single test, without remounting the sample. With the electro-mechanical method the real-time electrical resistance is measured in a very thin, conductive coating deposited on the brittle layer in which cracks develop across the width of the film. Simultaneously, the propagation of individual cracks is observed by optical microscopy. Real-time combination of both analyses in principle enables linking the fracture behavior (size, number and pattern of cracks) with the electrical resistance at a well-defined imposed strain.

With this 2PR method, the subcritical mechanical failure of a 150 nm thick SiN_x barrier layer was analyzed, as deposited on a 125 μm thick polyethylene naphtalate sheet (system 1). Its characteristic static failure time, as obtained from a Weibull analysis, was 0.10 s at a strain of 0.84% and 2.2 s at 0.77%. From the crack opening on reloading tests, an average internal compressive strain of 0.38% was deduced. In order to validate the results of the 2PR device, system 1 was also tested using two-plate bending (2PB), as described earlier. Results on characteristic failure strains as obtained with both methods for bending match very well and have similar accuracy. However, the option to assess tensile internal strains, together with the aforementioned advantages, renders the 2PR test the method of choice for testing brittle layers on polymer substrates. Comparison of system 1 with another barrier system (2), which only differs in processing conditions, indicates a considerable difference in time dependence of the characteristic failure strain, indicating the sensitivity of the resulting material properties on processing conditions.

1. Introduction

Multilayered structures comprising a polymer substrate on which a number of functional layers, such as transparent conductive oxide and diffusion barrier coatings, are deposited, have found widespread applications in flexible electronics and photovoltaic devices [1–3]. The functional performance of these composite structures is strongly dependent on their mechanical integrity, i.e., cohesion in each fragile layer and adhesion at their interfaces. During roll-to-roll manufacturing and use of these composite films, the multi-layered structures are subject to thermal-mechanical loads. Such an operation increases the risk of mechanical damage in these brittle layers and thus reduces the device performance and lifetime. Therefore, it is essential to characterize the mechanical failure behavior, like crack initiation and propagation, of brittle thin films and understand the failure mechanism under complex thermal-mechanical cycles to enable optimization of design and manufacturing of encapsulation solutions for flexible electronic devices.

In recent years, a great deal of research has been dedicated to the study of the mechanical failure of brittle thin films on a polymer substrate [4–16]. Three main techniques have been widely used to analyze the mechanical properties of thin brittle, hard films on soft substrates, namely nanoindentation and the related scratch test [17,18], the tensile fragmentation test [16,11], and the electro-mechanical two-point bending test (which, more properly would be addressed as the two-plate bending test (2PB), as we will do in the current paper) [6,16]. Among these methods the fragmentation test, which enables a direct observation of the failure process and thus an accurate determination of failure mechanism in brittle thin films, is the most commonly used one. The electro-mechanical 2PB test offers as key advantage an accurate determination of the critical onset strain with a localized application of the maximum strain and a continuous monitoring of the crack evolution, using a defined increase in electrical resistance as failure criterion [16].

* Corresponding author.
E-mail address: G.deWith@tue.nl (G. de With).
[1] Now at Holst Centre, High Tech Campus 31, 5656 AE, Eindhoven.

http://dx.doi.org/10.1016/j.tsf.2016.05.025
0040-6090/

This failure strain, as based on the bent state, is composed of (a) an internal strain $\varepsilon_{internal}$, defined as the residual strain between barrier layer(s) and the polymer substrate in a flat multi-layered structure, as induced by processing and by thermal mismatch, and (b) an intrinsic failure strain $\varepsilon_{intrinsic}$, which is the strain at failure of the barrier layer without any internal strain being present.

Other in-situ techniques have been adopted to measure stress and strain in brittle and ductile films during straining [19]. X-ray diffraction (XRD) techniques initially were used to measure residual stresses in thin films as well as thermal and process-induced strains [20–23]. Recently, XRD has been used to measure mechanically induced uniaxial [24,25] or biaxial [26] tensile strains of thin films. Combined strain measurements using XRD and digital image correlation were applied to characterize the early stage of the mechanical deformation of nanostructured thin films. The high accuracy allowed determining very small strains in both film and substrate [8]. Thus the initiation of plasticity and damaging in thin films can be assessed [26]. In-situ testing using scanning electron microscopy allows one to determine the fracture strain, crack initiation and subsequent propagation, buckling and delamination [27–29]. Atomic force microscopy (AFM) is often employed to determine the roughness of the surface of the thin film or the substrate, which is of great importance for determining the interfacial shear stress associated with adhesion in a multi-layered system [28]. With the capability of in-situ AFM imaging while loading the sample, the formation and growth of cracks and buckles were observed with information on depth and width of the cracks and the height and width of the buckles [30,31]. This provides valuable validation data when developing analytical models.

In this contribution our aim was to analyze, by electro-mechanical means, the failure characteristics due to bending for a barrier deposited on a polymeric foil. To apply bending, we employed a two-point rotation (2PR) technique, in which a strip is bent by applying a controlled rotation and positioning to the ends of the strip, resulting in a defined force and torque. This technique deviates from the two-plate bending (2PB) technique, as used by us before [16], in which a central part of a strip is bent between two approaching parallel plates, resulting in a torque-free configuration.

Our choice for 2PR was made because 2PR, especially when fully exploited, is more versatile for a number of reasons. Principal differences are:

1) Any desired strain distribution (e.g., between a distribution that is uniform across the sample and a distribution that is very much localized in the center) can be defined over a wide range, by properly adjusting the aspect parameters of a 2PR device; in 2PB the strain distribution in the bent zone is fully fixed and unique; note however, that this bent zone shrinks with the progress of approach of the parallel drive plates involved. The 2PB strain distribution can, in good approximation, be seen as a special case of 2PR (see also Section 2.2.3).
2) A 2PR device allows to impose a “negative” bending of the barrier, which allows crack closure, and provides a way to determine the internal strain, even when the production method of the barrier induced a tensile internal strain in the barrier layer in the flat state. In contrast, a 2PB device allows crack closure only in the case of a sufficiently large compressive internal strain, i.e., of typically more than 30% or 35% of the failure strain itself.

Additional advantages are:

3) A 2PR device, in contrast to a 2PB set up, allows the centre of the bent strip to be at an approximately fixed position, accessible for simultaneous microscopic observation of crack initiation and propagation. Moreover, the set-up has a limited building height in which the clamps rotate away from the objective lens so that the relevant test area can be observed completely.
4) Due to the smaller specimens size that can be used without reduction of the characteristic tested area, the 2PR design is more suitable than the 2PB setup to be operated in a climate box for temperature and humidity control.
5) Mounting a sample in 2PR is typically done with the sample in a flat orientation. On the other hand, mounting in a 2PB facility requires a considerable bending of the sample, which may damage a sample with an internal tensile strain.

In comparison to the conventional mechanical testing method, such as three-point bending or four-point bending, the two-point rotation device exhibits significant advantages when testing thin film materials. In the three-point bending method only small sample deflection is allowed, which means that for flexible samples like thin films on polymer substrates, mechanical tests can only be performed on a limited sample length. This restriction reduces the size of the tested area on the sample. These methods are also experiencing electrical contact problems when combined with elctrical measurements. The two-point rotation test can be performed on significantly longer samples providing a larger tested area, which is of importance for the prediction of failure in large size films as used in production.

The barrier layer of our interest, on a polymeric foil, was tested systematically with the 2PR electromechanical facility. In order to be able to compare 2PR results with our previous 2PB results, we mimicked the 2PB conditions within the 2PR facility. For validation, these results were then compared with results of additional 2PB tests. In this paper the focus is on the electrical detection of fracture failure in barrier layers using the 2PR method. While an example of optical crack detection will be given, a detailed discussion of the combined optical and electrical detection and analysis of cracks will be presented in a forthcoming paper.

2. Experimental

2.1. Materials

The samples used in this paper were similar in composition to the ones described in [16] but with different, proprietary, processing conditions. A non-stoichiometric SiN_x film with a typical thickness of 150 nm was deposited by low-temperature plasma-enhanced chemical vapor deposition on a polyethylene naphthalate (PEN) substrate with a thickness of 125 μm. A thin conductive layer of indium-tin-oxide (ITO) with a nominal thickness of 10 nm was sputtered on top of the SiN_x layer as an electrical probe. The sputtered ITO layers have a sheet resistance of typically about $R_{\square} = 1000\ \Omega/\square$. It was shown in [14] that the thin ITO layer does not affect the failure behavior of SiN_x beneath, so that it can act as an effective probe to monitor the fracture failure in the SiN_x layer.

In order to eliminate the bias in analyzing data caused by any manufacturing variability in the samples, 16 sheets in size of about $150 \times 150\ mm^2$ were produced. From these sheets a large set of strips, 220 strips, with a width of 10 mm were cut along the transverse direction, which is perpendicular to the machine direction in a stretching process of the polymer, and each strip was coded to be able to track its origin. Samples used for electrical and optical measurements using two-point rotation were selected from this batch using a random selection procedure, in which a random permutation of the integers from 1 to 220 is generated, and the sample of each measurement was taken according to the randomized order. The samples were tested in the 2PR device for their electro-mechanical response, while simultaneously carrying out optical microscopy observations of crack growth. For these measurements, sample strips with a typical length of 40 mm were used. All measurements were conducted at 21 °C and 50% relative humidity. Prior to any measurement all samples were equilibrated at these conditions for more than 15 days.

Using the same batch of samples, a complementary set of 2PB tests were carried out using the facility described in [16], again employing a random selection procedure and using the same pre-conditioning and

measurement conditions. For 2PB testing, samples with a length of 150 mm were tested.

2.2. Mechanical two-point rotation device

2.2.1. Schematic

The in-house built two-point rotation (2PR) device was designed for testing the mechanical failure behavior of brittle thin films on a compliant substrate. The computer-controlled motor-driven rotation stages have a limited building height to allow microscopic observation, simultaneous with electrical resistance measurements along the strip, for which purpose the strip clamps are equiped with electrical contacts (see below).

The basic geometry of the 2PR facility is shown schematically in Fig. 1. A strip of material is fixed at both ends in clamps mounted symmetrically on motor-driven rotators. The distance between the two clamps in the neutral state (rotation angle $\alpha = 0°$) is defined as the clamped sample length b. The distance between the centers of the rotators is a. The distance between the neutral plane of the sample strip and the plane through the rotation axes is c. Upon loading, the two rotators rotate symmetrically over a predefined angle α at a predefined angular velocity, by which the sample strip is mechanically loaded in tension at the outer surface and in compression at the inner surface. Hereafter we will describe the relation between the rotation angle of the clamps and the actual strain in the brittle layer of the bent sample, first for rotation to a uniform strain and thereafter for rotation to a strain distribution.

2.2.2. Realizing a uniform strain distribution

With an appropriate choice of the span ratio b/a and the rotation angle α, a circular profile will be applied along the whole sample strip between the clamps. This condition can be found by demanding the arc length to be equal to the clamped sample length b, i.e.,

$$b = 2r_0\alpha \tag{1}$$

where r_0 is the radius of curvature of the circular arc. The span ratio b/a for which the bent strip in Fig. 1 has a circular shape is given by

$$\frac{b}{a} = \frac{1-\cos\alpha-2\frac{c}{a}\sin\alpha}{\frac{\sin\alpha}{\alpha}-\cos\alpha} \tag{2}$$

This equation shows that the ratio b/a for a constant curvature depends on the deflection angle α and the relative offset distance c/a. Fig. 2 shows the span ratio b/a as a function of the defection angle α in a range of $0 \le \alpha \le \pi/2$ (i.e., between 0° and 90°) required for a constant curvature. For the offset $c = 0$, which represents the situation where the rotation axes coincide with the neutral plane in the sample, this figure clearly shows that a uniform curvature is obtained within a limited

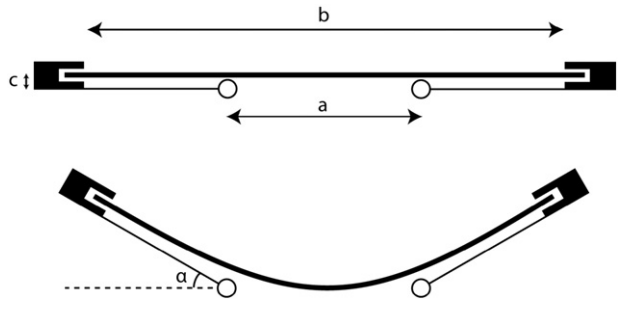

Fig. 1. Schematic illustration of the two-point rotation bending setup in the neutral state and when rotated over an angle α. The thick line represents the test strip with a clamped length b. The clamps are connected to the rotation axes that have a mutual distance a. The neutral bending plane in the sample has an offset c with the plane through the rotation axes, depending on design of the clamps and the sample thickness.

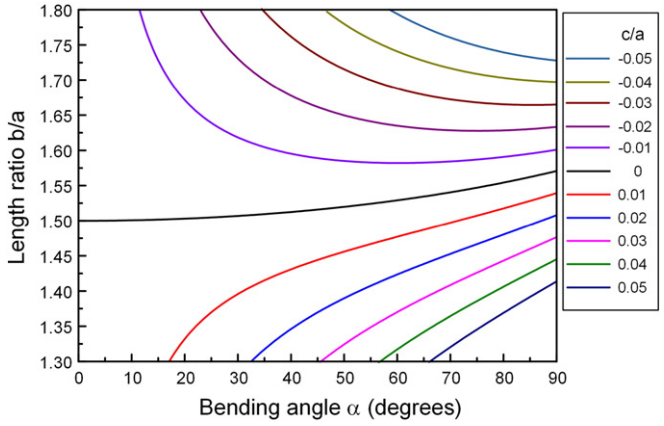

Fig. 2. Span ratio b/a required for a constant curvature along the sample strip for various c/a offset values.

span ratio range, i.e., $1.50 \le b/a \le \pi/2$, and that the actual span depends on the deflection angle α. In previous work [32], where it was the intention to have an approximate uniform curvature of the sample strip, a span ratio b/a of about 1.50 was used in the bending jigs. A small deviation in local curvature exists at different bending angles but is limited to within an acceptable range. Fig. 2 also shows that a small offset distance c (or ratio c/a) results in significantly different b/a ratios for constant curvature.

2.2.3. Realizing a non-uniform strain distribution

In our 2PR set-up we used span ratio b/a deviating from the values depicted in Fig. 2 in order to induce a non-uniform curvature with the largest deformation in the center of the sample strip so that cracks are expected to initiate and propagate predominantly at this location, like in the case of 2PB testing. Numerical methods were used to evaluate the local curvature on the bent plate as function of α, b/a and c/a and to select a proper value of the span ratio b/a.

In the bent state the plate is assumed to be in static equilibrium. At both clamps, a moment M and a force F are applied to the plate. They are equal in size and opposite in direction from symmetry considerations, as shown in Fig. 3. The force balance requires the force for every position x on the plate to be the same, i.e., $F(x) = F$. From the moment balance it follows that

$$M(x) = M + F \cdot y(x) \tag{3}$$

Due to the bending moment, the sample is curved and the curvature $\kappa(x)$ at every position x on the plate is determined by the moment $M(x)$ and the flexural rigidity D, i.e.,

$$\kappa(x) = \frac{M(x)}{D} \tag{4}$$

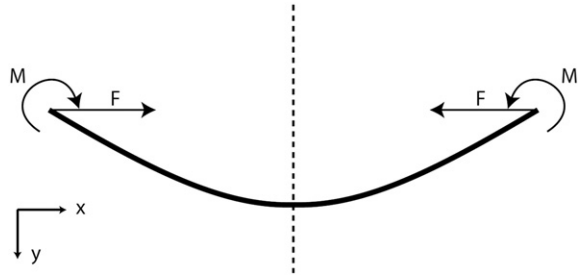

Fig. 3. Applied force and moment to the bent plate in static equilibrium. The origin of the coordinate axes is at the left clamp.

For a plane curve given explicitly as $y = f(x)$, its curvature is.

$$\kappa(x) = \frac{y''(x)}{\left(1 + y'(x)^2\right)^{3/2}} \tag{5}$$

Combining Eqs. (3), (4) and (5), an equation in terms of the applied bending moment M and force F returns, from which the shape of the bending curve can be determined, i.e.,

$$\frac{M}{D} + \frac{F}{D} \cdot y(x) - \frac{y''(x)}{\left(1 + y'(x)^2\right)^{3/2}} = 0 \tag{6}$$

For a beam of uniform height h and width w, the flexural rigidity D is described as.

$$D = \frac{Ewh^3}{12(1-\nu^2)} \tag{7}$$

where E and ν are the Young's modulus and Poisson's ratio, respectively.

The differential equation (Eq. 6) describes the shape of the bent plate and numerical techniques are used to solve it. In this second-order differential equation two boundary conditions should be specified, normally taken as: (i) by imposing a starting angle α, the slope at the clamp is $y'(0) = \tan\alpha$; and (ii) the position of the clamp remains as $y(0) = 0$ in bending. However, in the current set-up the moment M and force F are not known, and thus the shape has to be determined by adopting another set of boundary conditions specified by a, b and c. From symmetry considerations only half of the bent plate is taken into consideration and thus 2 l is defined as the rectilinear distance between the clamps in a bent state. According to the geometry of the set-up shown in Fig. 1, one can see that.

$$l(\alpha) = \frac{b-a}{2}\cos\alpha + \frac{a}{2} - c\sin\alpha \tag{8}$$

The first boundary condition is that at the center of the bent plate $\alpha = 0$, i.e., $y'(l) = 0$. The second boundary condition is formed by constraining the length of the plate between the clamps equal to b so that

$$b = 2\int_0^l \sqrt{1 + y'(x)^2}\,dx \tag{9}$$

The actual shape of the bent plate depends on both the length ratio b/a and the offset distance c/a. Numerical studies show that, slightly depending on the rotation angle α, an almost constant curvature is obtained for the span ratio $b/a = 1.52$, which is in accordance with the model results in Fig. 2. The magnitude of strain at the clamping positions significantly depends on the span ratio, i.e., it is about zero when $b/a = 2.0$ and much higher for much lower span ratios. For the present set-up, a length ratio $b/a = 2$ is used to obtain the largest local deformation in the center. The values of the parameters a, b, c and α in the present two-point rotation system are measurable, so the local curvature along the sample strip with the aforementioned specific geometry can be determined accordingly.

Young's modulus E, Poisson's ratio ν, the height (thickness of the sample strip) and width of the beam (width of the sample strip), h and w, respectively, are known. As an initial guess the ideal circular arc, represented by $F = 0$ and $M = -(D/l)\sin\alpha$, is used from which the resulting curve is calculated and the two boundary conditions, i.e., the clamped length of the sample b as mentioned in Eq. (9) and the value of $y'(l)$, could be determined. Then F and M are varied in order to find the proper length b meanwhile satisfying $y'(l) = 0$. The resulting bent plate shape $y(x)$ for $b/a = 2$ is shown in Fig. 4 (a). The

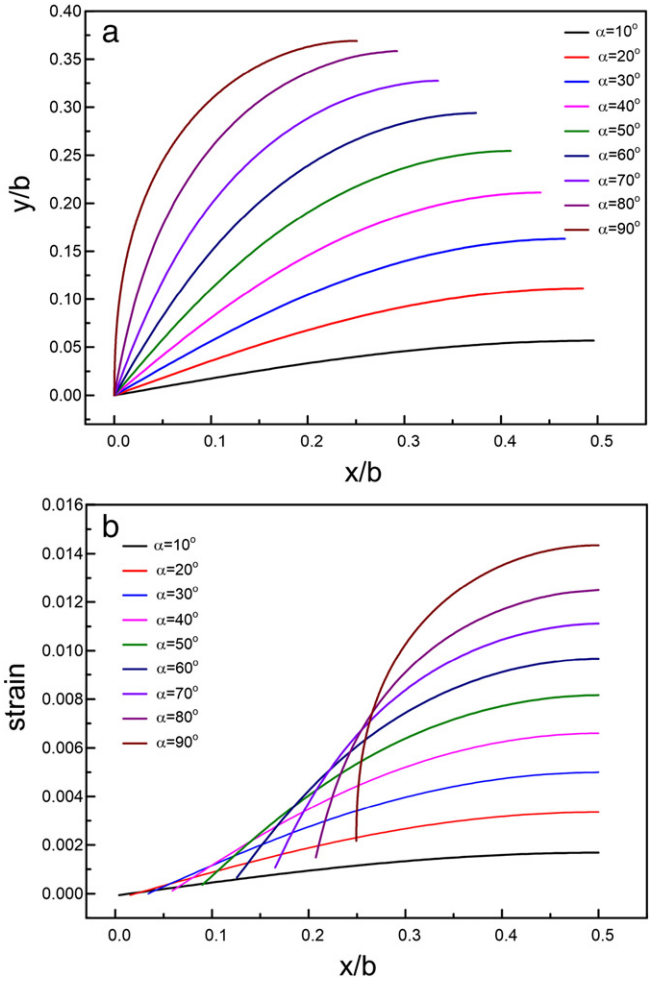

Fig. 4. (a) The bending shape and (b) strain profile in deflection angle α from 10° to 90° when the span ratio $b/a = 2$ and $c = 0.017$ mm.

local curvature r along the plate leads to an locally applied strain ε_a at the upper sample surface given by

$$\varepsilon_a = h/2r \tag{10}$$

Resulting distributions of ε_a values along the plate for a range of rotation angles are shown in Fig. 4 (b).

The 2PB method (Fig. 1 in [16]) can be seen as a specific realization of the more general 2PR method; in fact, when the deflection angle in 2PR is $\alpha = 90°$. In that case, the 2PB plate-plate distance corresponds to the distance between the rotation axes a in 2PR. Because in a 2PB test the sample is flat at the location of the contact point, we know that $M = 0$ at that point. A zero torque condition at the clamps at $\alpha = 90°$ in 2PR corresponds to a well-defined b/a ratio. From the analytical model for 2PB as discussed in literature [33,34] this b/a value in 2PR can be deduced to be 2.18 [34]. Thus, at b/a values well beyond 1.5 the highest curvature and largest strain are at the center of the bent plate. At a deflection angle $\alpha = 90°$ and $b/a = 2.18$, 2PR generates exactly the 2 PB shape.

2.2.4. Implementation

The two-point rotation set-up is shown in Fig. 5. A rectangular sample strip is clamped at the clamp plates fixed to the two rotators. The fixed face of the clamps is a glass plate with a copper electrode deposited on it. The sample strip is positioned with the conductive layer facing the electrode. The removable face of the clamp is an aluminum plate that is screwed to the fixed face to ensure good electrical contact

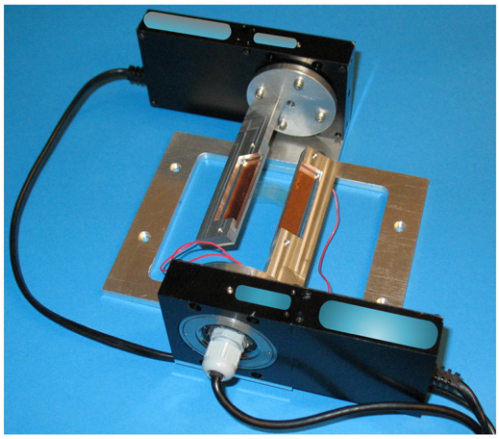

Fig. 5. View of the two-point rotation set-up.

between copper electrode and sample. In order to ensure an accurate measurement of the crack-induced strip resistance increase over a wide range, without range switches of the meter during the measurement, a stable 10 V DC was imposed to the sample with initial resistance R_0. A fixed resistance of $\approx 10R_0$ was put parallel to the sample and a fixed resistance of $\approx R_0$ in series with the sample, in order to keep the recorded resistance finite throughout the experiment. A LabView computer program was used to control the sample deformation and to register the rotation of the motors and the voltage drop over the sample.

The rotation angle controlled by the computer was based on the prescribed highest strain $\varepsilon_{a,c}$ at the plate surface, i.e., at the center of the sample where the local radius of curvature has the value r_c. Combination of Eqs. (1) and (10) results for the centre of a plate of uniform height h in:

$$\varepsilon_{a,c} = \alpha(h/b)(r_0/r_c) \tag{11}$$

The values of r_c were based on numerical results, using the proper values for a, b and c. Because the symmetry axis of the equipment is located 45 μm above the clamp faces, the distance c is 17 μm for a 125 μm foil. The other geometric parameters of our 2PR device are $a = 10.29$ mm and $b = 20.59$ mm. By a least-squares fitting procedure to numerical results, the relation between r_0/r_c and α was found to be

$$r_0/r_c = c_0 + c_1\alpha^2 + c_2\cos\alpha \tag{12}$$

with parameters $c_0 = 1.659$, $c_1 = 1.85 \times 10^{-5}$, and $c_2 = -0.088$ as determined for the current geometry. Combining of Eqs. (11) and (12) defines the relation between α and $\varepsilon_{a,c}$. Based on this, strains and strain rates were imposed.

Using this relation between rotation angle and strain in the center of the plate, any strain - time profile can be imposed, within the limits for the rotation speed of the motor. We conducted tests in two modes, either with a strain linearly varying with time ("dynamic loading") or with a constant strain ("static loading") in which the strain in the beginning of the test was quickly raised to the required static level. It is obvious that the time needed for raising the strain to the static level induces an uncertainty in time when studying the crack length or resistance as a function of time in the loaded state. Practically speaking, the static mode is especially useful for studying lower strain levels with correspondingly lower crack growth speeds. When studying higher strain levels, this aforementioned uncertainty in time becomes unacceptably large; in this case the dynamic mode is appropriate (note also that using the dynamic mode for low strain levels is impractical in view of the excessive testing times needed). The results obtained using both modes can be well compared, as discussed in [16].

3. Results and discussion

3.1. Crack opening and closure

We start with a discussion of typical features of the evolution of electrical resistance during repetitive loading and unloading of a sample in 2PR and an example of how growing cracks can in principle be analyzed. Thereafter, a detailed analysis of barrier failure, as probed electrically, will be given.

In our 2PR device, two rotational speeds of the sample clamps, i.e., 0.5°/s and 10°/s, were used, corresponding to strain rates of $0.874 \times 10^{-4}\,s^{-1}$ and $17.5 \times 10^{-4}\,s^{-1}$, respectively, resulting in a linear change of strain with time (assuming that the sample behaves elastically). The applied strain profiles and an example of a measured resistance curves are shown in Fig. 6. Upon loading, the resistance enhances dramatically once fracture occurs. Upon unloading, the hysteresis in resistance indicates that cracks remain open in the layer for a while. When the applied strain is lowered to below the internal compressive strain in the layer, the cracks do close and, as a consequence, the resistance drops to approximately its initial level. Crack closure can be affected by many local factors and thus behaves differently for each single measurement. To some extent, it reflects the level of internal strain in the layer that leads to the crack closure during unloading.

As can be observed in Fig. 6 (b), the failure strain is strain rate dependent. This was also observed and discussed in previous work [16]. Subcritical crack growth (SCG) theory is used for the interpretation of the

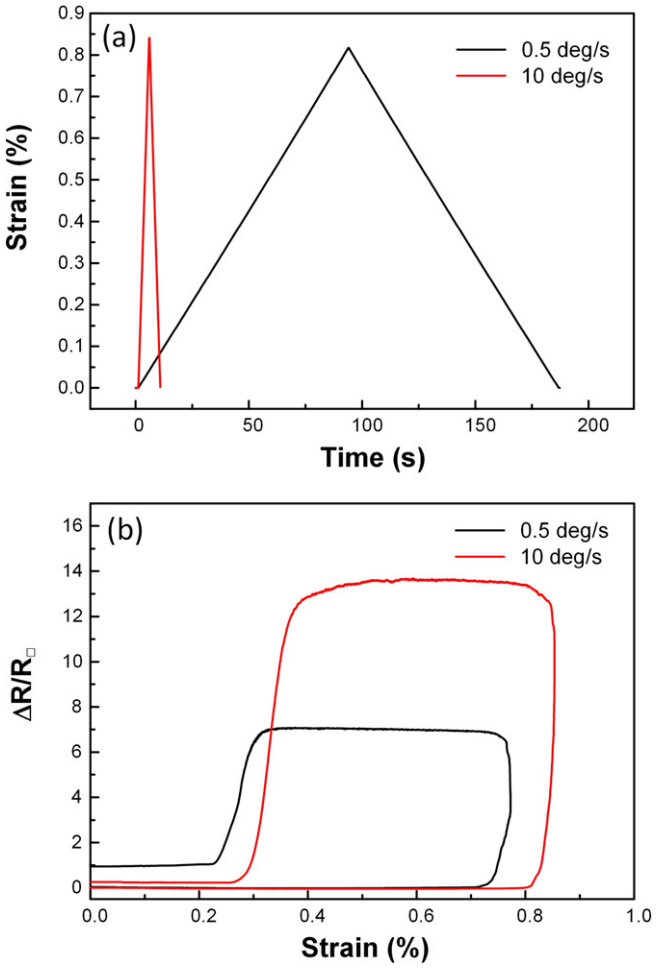

Fig. 6. Strain profiles and electrical resistance at two rotational velocities for the 2PR device, with corresponding strain rates of 0.874×10^{-4} (black) and $17.5 \times 10^{-4}\,s^{-1}$ (red).

data. The crack velocity v is described as $v = AK_I^n$, with the SCG exponent n representing the susceptibility of the material to stress corrosion. The parameter A is a constant, depending on the environmental conditions and the material. The stress intensity factor $K_I = Z\sigma h^{1/2}$, with σ the applied stress (Z is a geometry factor that is a function of the film thickness h for channeling cracks, in contrast to case of bulk materials where it is a function of the crack length c) [16]. On the assumption that barrier and supporting material behave elastically, the crack velocity also depends to the strain ε in the barrier according to $v \propto \varepsilon^n$. This is the explanation for the fact that the high strain rate resistance only shows a extremely small increase (non-visible in Fig. 6 (b)) below a strain of 0.8%, while the low strain rate resistance already deviates visually from the base line at a strain of 0.72%.

In Fig. 7 examples are shown of the resistance during two loading and unloading cycles, both for 2PR and 2PB (the rates in 2PB were 0.833×10^{-4} and 16.7×10^{-4} s^{-1}; details on how this rate was implemented are given in [16]). In all cases, in each cycle the strain was raised linearly with time up to its maximum and then linearly reduced either to the lowest attainable level (2PB) or to zero (2PR). In stage 2 in Fig. 7 (b) we see that the crack growth speed again depends very sensitively on the imposed strain. Thus, during unloading (stage 3), at first a crack continues to grow but as soon as the strain is below ≈0.7, crack growth virtually ceases completely and the resistance stays fully constant, until cracks start to close at a strain of ≈0.3 in stage 4. Ideally, the resistance falls back to its starting level. However, crack closure is often not complete. Possible causes are that pieces of debris reside between the faces of a crack or that the barrier locally delaminates from the polymeric carrier. Even when the resistance does not return fully to its initial level, still an estimate of the closure strain can be made, be it less accurately. For the second loading cycle again a resistance increase appears due to opening of cracks formed during the first cycle. Usually this opening is at a strain that is slightly above the crack closure strain of the first loading cycle. The difference in strain between stages 4 and 7 in Fig. 7 (b) is typical but can be smaller; the difference between stages 4 and 5 in Fig. 7 (a) is exceptionally large. The origin of this phenomenon is not clear but possible causes are adhesion between the faces of a crack and relaxation processes in the polymeric sheet. As long as the strain imposed in the second loading cycle stays well below the strain at which growth became noticeable during the first cycle, the cracks appear not to grow, as registered by the resistance (stage 5 in Fig. 7 (a)). Once the strain arrives at that strain level, growth is also noticed in any next cycle, e.g., stage 6 in Fig. 7 (a). Note that in the 2PR case in Fig. 7 (b) such growth in the second cycle did not occur because the strain in the second cycle was only raised up to 0.4.

As reported in our previous work [16], as well as by Vellinga et al. [14], the resistance curve of the unloading stage contains important information on the internal strain in the SiN_x film. One of the motivations for developing the 2PR tool was to overcome the missed closure during unloading in 2PB. The 2PR method allows access to bending angles from −90° to +90°, so that a wide range of strains can be applied to the sample, thus allowing both tensile and compressive loading in a single test without demounting. This is illustrated in Fig. 7 (b), where the resistance response of imposing strain on a SiN_x film with a compressive internal strain of ≈0.38% is shown for the 2PR method. The crack closure during unloading can be monitored fully and, if needed, negative strains can be monitored as well by imposing negative rotation angles. For comparison, in Fig. 7 (a) a corresponding result is shown for the 2PB method. It can be clearly seen that crack closure (stage 4) can not be completed in 2PB due to the lower limit of the accessible strain range, typically at 0.25% for the current sample geometry.

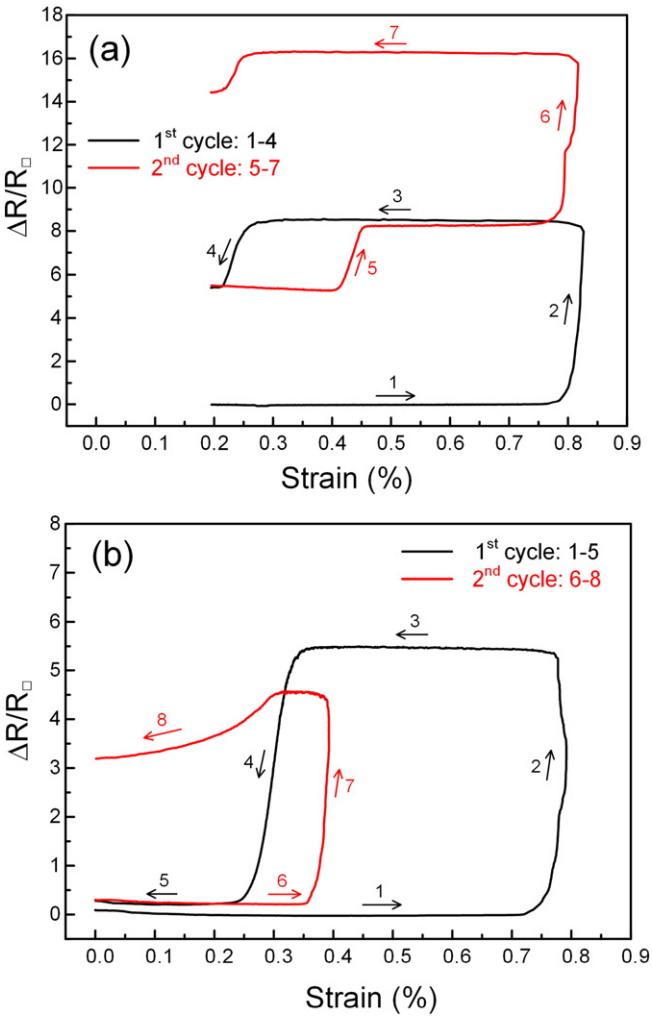

Fig. 7. The change of electrical resistance by imposing strain on a SiN_x film with low compressive internal strain, both with (a) the 2PB and (b) the 2PR method. Two loading-unloading cycles were carried out for each method.

3.2. Optical crack observation

2PR allows optical observation of fracture in brittle thin films. This feature of our 2PR device is especially useful when applying a constant strain. In case of dynamic loading (constant strain rate) the crack tip speed increases so fast in such a short time interval that taking useful snapshots is cumbersome. We will illustrate the method with two examples at constant strain. In Fig. 8, cracks started from the damaged sample edge (containing small cracks at an angle of ≈60° due to

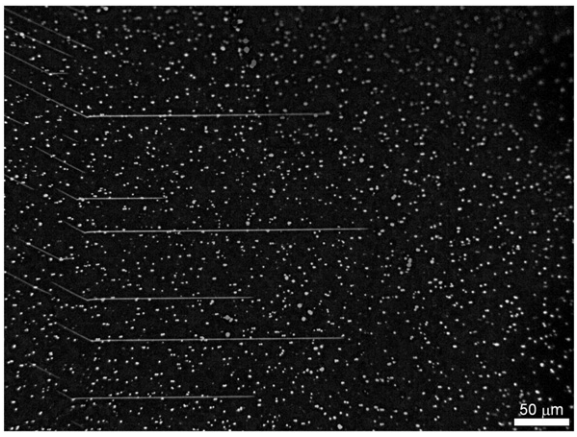

Fig. 8. Optical observation of fracture in a SiN_x layer at an inposed strain of 0.70%. At the cutting edge at the left, thin cracks appear at ≈60° to the edge. Their tips act as starting locations for cracks, normal to the imposed tensile strain.

cutting), similar to previous results [35]. It appears that the electrical resistance measurement is not sensitive enough to detect these short initial cracks in the film (because the resistance increase due to a small crack is very small as it scales with the square of the crack length [38]; additionally, distinguishing the effects of the growth of a newly formed small crack from that of the opening of a crack made during the preparation of the sample is cumbersome). Hence, optical observation provides valuable information on the early stage of fracture, such as size, number and distribution of the cracks at a specific applied strain. Once a significant increase in electrical resistance is measured, the real-time combination of both types of measurement enables one to link the fracture behavior (size and number of cracks) with its associated resistance, as can be seen in Fig. 9, where the crack growth over a time interval of 12 s is shown in micrographs, together with the registered increase of resistance in a system 1 sample for a constant strain of 0.71%.

Summarizing, the 2PR method allows combined optical observation and electrical measurement over a wide range of applied strains, facilitating mechanical characterization of brittle thin film.

3.3. Electro-mechanical measurements of barrier failure

Failure of a barrier layer can be defined in many ways. From the point of view of growing a single crack, a logical criterion is that the crack has traveled over a specific fraction φ of the full sample width w. In that case a dynamic failure strain of the thin film

$$\varepsilon_{f,d} = \left[\frac{\varphi w(n+1)}{AZ^n\sqrt{h}^n}\right]^{\frac{1}{n+1}} \dot{\varepsilon}^{\frac{-1}{n+1}} \tag{13}$$

is expected [16]. This rationalises that in Fig. 6 (b) the failure strain at high rate tends to be higher than at low rate. In addition, the SCG exponent n can be determined using Eq. (13) for the prediction of the service life time of barrier coatings.

It is important to avoid crack-induced electrical field distortions in the sample near the clamps because this complicates the interpretation of resistance increase significantly. Since the center of the sample experiences the highest strain, any distortion of the electrical field in a sample is always located in the central area of the sample, and because our samples are relatively long, the distorsion is always far away from the clamps. In fact, such distorsions have already vanished over a distance along the length direction that is smaller than the full sample width w [36].

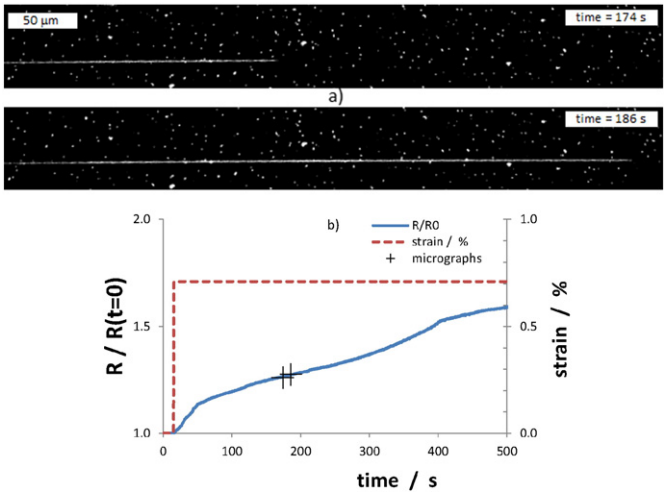

Fig. 9. Crack growth in a SN_x barrier layer at an imposed constant bending strain of 0.71%, as registered both microscopically (Fig. a) and electrically the resistance of the thin ITO probe layer on top of the barrier layer (Fig. b). The two micrographs are taken at the times indicated by crosses in Fig. b.

The resistance of a single crack, far away from any other crack, can be seen as an increase in effective sample length [38]. This suggests to scale the crack-induced resistance increase by the resistance of a crack-free sample that is as long as it is wide, i.e., with the resistance that is conventionally called the sheet resistance $R_\square$. This scaled resistance is evaluated on the basis of measured data using.

$$\frac{\Delta R}{R_\square} = \frac{R - R_0}{R_0}\frac{b}{w} \tag{14}$$

where b is the sample length, w is the sample width, R and R_0 are the final and the initial resistances, respectively. In the present study $\Delta R/R_\square = 1$ is chosen as the length-independent failure criterion, the value chosen being based on arguments given below. Accordingly, in a dynamic test, in which the strain is linearly increasing, the moment the criterion is met, defines the dynamic failure strain $\varepsilon_{f,d}$ and the dynamic failure time $t_{f,d} = \varepsilon_{f,d}/\dot{\varepsilon}$; obviously both values will be functions of the applied strain rate. When a constant strain is imposed instantly, the criterion is used to define the static failure time $t_{f,s}$, which will depend on the applied strain. Both failure strains are within the SCG theory linked to each other [16], according to:

$$t_{f,d} = (n+1)t_{f,s} \tag{15}$$

The failure criterion chosen corresponds to the resistance effect caused by a single edge crack tip that has traveled across 77% of the sample width [36]. Regarding the different sample dimensions, the criterion corresponds to a resistance increase of about 48% for the 40 mm long 2PR samples (clamped part is $b = 21 \pm 0.3$ mm) and of about 7.5% for the 150 mm long 2PB samples (clamped part is $b = 133 \pm 0.3$ mm).

The choice of criterion $\Delta R/R_\square = 1$ was based on results given in [16], in which 2PB with 150 mm long, 10 mm wide strips was carried out and in which 2%, 10% and 20% resistance increases were compared as criteria for failure. Results and trends in results were found to be very similar, be it that dynamic failure strains of course were larger for the larger resistance increase criterion. In the current paper we want to use an optimum criterion, based on two considerations. First, the resistance increase should be large enough for an accurate determination of resistance increase. Second, a crack should preferably not have grown over almost the full width of the strip. In our 2PB tests, a single crack originating at the side edge causes a resistance increase of 2%, 10% and 20% when it has grown over 40%, 77% and 92% of the strip width [36]. A resistance increase of 7.5%, as caused by a crack of 77% of the width, appears a fair estimate of the optimum criterion. Note that microscopic observations revealed that usually many cracks appear simultaneously. No theoretical link between the many-cracks configuration and electrical resistance does exist as yet (except for short cracks [38]. Hence, we have to stick to the criterion originally based on the single crack idea. For the case of multiple cracks, without knowledge about relative position of cracks and crack density, the only thing that can be said is that now the failure criterion corresponds to an average crack length/width ratio that is smaller than 77%.

3.4. Weibull statistics and characteristic failure strains

Failure strains of individual samples vary in value, as dealt with in the theory of Weibull. In order to determine the characteristic failure strain (representing the location of the strain distribution), for a specific condition (e.g., a chosen dynamic strain), 20 samples were tested. A two-parameter Weibull distribution was used to describe the fracture probability P of the brittle thin-film barrier layer. It is given by

$$P = 1 - exp\left[-\frac{A}{A_0}\left(\frac{\varepsilon}{\varepsilon_0}\right)^m\right] \tag{16}$$

where m is the Weibull modulus which describes the homogeneity of the defect distribution for a given area A. The parameter ε_0 is the characteristic failure strain (in the case of imposing a dynamic strain, the characteristic dynamic failure strain $\varepsilon_{0,d}$) which is obtained from

$$\ln\left[\ln\frac{1}{1-P}\right] = m\ln\varepsilon - m\ln\varepsilon_0 + \ln\frac{A}{A_0} \tag{17}$$

as the strain at $P = 0.6321$. In practice, to estimate the Weibull parameters m and ε_0, the data points have to be ordered and, using least-squares methods, their probability estimated. This is normally done by using an estimator based on the rank number and the number of samples. It has been shown [37] that the estimator

$$F = (i-0.5)/N \tag{18}$$

where i is the rank number of the data point and N the number of samples used, is both the most accurate and the least-biased of the regularly used estimators. An approximate estimate of the reliability of ε_0 can be made by $s(\varepsilon_0)/\varepsilon_0 = 1/m\sqrt{N}$, where $s(\varepsilon_0)$ and n denotes the standard deviation of ε_0 and the total number of specimens respectively.

The failure probability as a function of dynamic strain is plotted in Fig. 10 for both the 2PR and 2PB tests. The characteristic dynamic failure strains found in 2PR and 2PB match very well with each other. They have both a value of ≈0.77% at the low strain rate level and of ≈0.84% at the high strain rate level, as shown in Fig. 11 together with error bars for their standard deviations of the characteristic failure strain.

The Weibull modulus is $m = 49$ as deduced from both 2PR and the 2PB tests, whilst the SCG exponent is $n = 37$ as deduced from 2PR tests and $n = 38$ from the 2PB tests. From electrical resistance curves on reloading, the internal strain in the barrier layer was determined. The average value from 2PR tests is 0.38%, while from 2PB a value of 0.39% was obtained. Some caution is justified here because in the case of 2PB for about 30% of the samples no proper crack closure and reopening could be registered. These cases were left out of the calculation of the internal strain average. These results show that with the 2PR and 2PB methods the same parameter values are obtained and, hence, these two devices produce rather comparable results. From the material point of view, we conclude that these data are reliable characteristics of this material. It is interesting to compare the failure characteristics of the current SiN_x barrier layer ("system 1") with those of the barrier layer studied in [16] that was made of the same material but with deviating processing conditions ("system 2"). System 2 was tested in 2PB both under dynamic and under static load conditions. To compare them conveniently, all characteristic dynamic failure data were, using Eq. (15), converted into static equivalents according to the SCG theory, using the $\Delta R/R_\square = 1$ criterion in all cases.

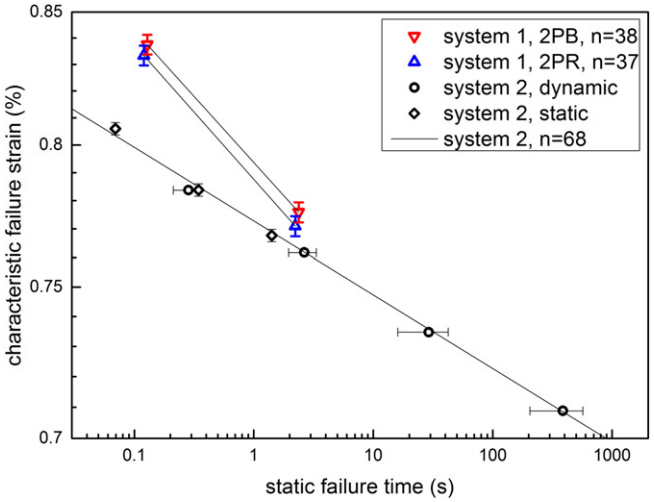

Fig. 11. The characteristic failure strain as a function of the characteristic static failure time for SiN_x layers produced by different processing procedures, as plotted on logarithmic scales. The material tested in this paper (system 1) was analyzed by both 2PR and 2PB. The 2PB results for system 2 were taken from the extensive analysis in [16]. The error bars indicate the standard deviations in the failure strains and times.

The resulting data for system 1 are shown in Fig. 11. At equal static failure times, the measured difference in characteristic static failure strain between 2PB and 2PR is about 0.005% strain units. The characteristic static failure strains as obtained from both 2PB and 2PR also follow the same trend with time, as reflected by a comparable SCG exponent n, which further confirms the consistency of the results and the compatibility of these two methods. In Fig. 11 also the results for system 2 are shown [16]. It can be seen that by combining the results from dynamic and static strain tests, characteristic failure times over a wide range, more than four decades, can be accessed. More importantly, all data points from both dynamic and static measurements fall on one single curve, obeying a power law between characteristic failure strain and failure time. Note that the value of the SCG exponent n of the previously studied barrier system (system 2) is 68, which is significantly higher than the value for the system tested here ($n = 38$). The reason is simply that for system 2 a different processing procedure was used, greatly affecting the quality of the barrier in terms of the internal strain and the surface quality of the polymer substrate. However, the applicability of the approach will be clear. Based on this result, we are confident to draw a straight line between the two data points from two strain rates in the present testing results.

When comparing 2PR with 2PB, each method has one or more advantages. On the one hand, 2PB allows fast clamping and is thus efficient when testing a large batch of samples for a statistics-based determination

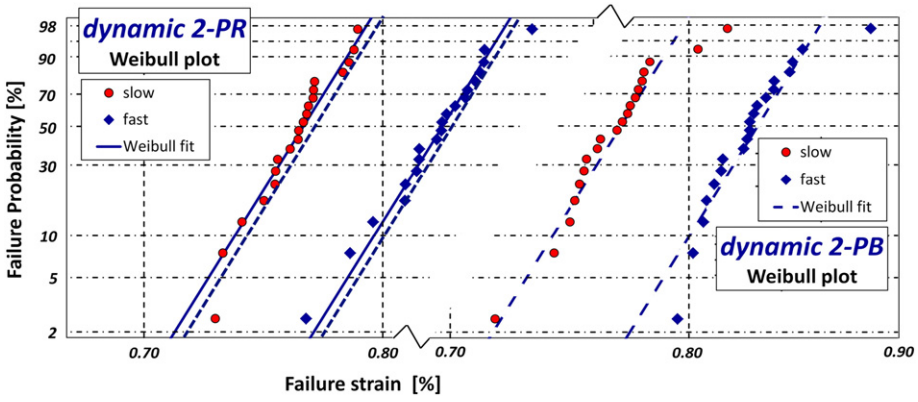

Fig. 10. Weibull analysis of the dynamic failure strain for a slow and a fast linear increase of strain. At left two-point rotation data, at right two plates bending data, together with their Weibull fits (dashed lines). For comparison, the Weibull fit of 2PB is reproduced at the right.

of the characteristic failure strain. On the other hand, an advantage of the two-point rotation method is that it allows combining electrical crack detection with optical microscopy for a more detailed investigation of crack propagation. Another advantage is that the 2PR technique allows mounting the sample without applying any strain, while the 2PB technique requires bending the sample to some extent during mounting (typically raising the strain in the direction of the tensile state over about 0.25% for the present sample geometry). Such bending during mounting in 2PB may damage fragile samples, i.e., samples with a tensile or a small compressive internal strain. In addition, the 2PR technique allows to study the closure of cracks in layers with a tensile internal strain by using negative angles, resulting in a (compensating) compressive applied strain. For the 2PB method it is evident that crack closure of layers with an internal compressive strain of less than ≈0.25% will be inaccessible. Thus, full testing of films with any tensile or a small compressive internal strain can practically only be conducted in 2PR but not in 2PB. Together with the aforementioned advantages, this renders the 2PR test the method of choice.

4. Conclusions

A two-point rotation (2PR) bending tool was developed to characterize fracture failure in brittle thin films on polymer substrates, using both electrical and optical observation. The bent shape and local strain along the bending curve at each deflection angle were numerically determined. For the application of this bending tool, an analytical expression was employed to determine the maximum imposed strain at each deflection angle. Examples are given of how this method can be used for optical crack detection and for the determination of the internal strain from an reloading test.

Using a 2PR device, systematic electrical measurements were performed on a 150 nm thick SiN_x barrier layer deposited on a 125 μm thick polyethylene naphtalate sheet, covered with a 10 nm indium tin oxide layer as a electrical resistance probe (system 1). The characteristic static failure time as obtained from a Weibull analysis was 0.10 s at a strain of 0.84% and 2.2 s at 0.77%. From crack opening on reloading tests, an average internal compressive strain of 0.38% was deduced. In order to validate these results, system 1 was also tested in 2PB. Results on characteristic failure strain ε_0, Weibull modulus m and subcritical crack growth exponent n as obtained with both methods match very well, while both methods result in similar accuracy. However, the 2PR test is much better suited then the 2PB test for the determination of internal strain from reloading tests, because from a considerable fraction of the 2PB tests no internal strain value could be deduced.

Results were compared with 2PB results from previous work on another barrier (system 2) that only differed in processing conditions. A Weibull statistics-based study of the failure strains using these two types of systems shows consistent results with respect to characteristic failure strain ε_0, Weibull modulus m and subcritical crack growth exponent n. However, a considerable difference in the time dependence of the characteristic failure strain was found, indicating the sensitivity of the resulting material properties on processing conditions. While the two methods have shown to yield the same results, the 2PR method offers the additional advantages of allowing simultaneous electrical and optical measurements during crack propagation. Moreover, the 2PR method gives access to the full range of bending angles between −90° and +90°, resulting in tensile and compressive loading in a single test, allowing to determine either compressive or tensile internal strain in the layer.

Acknowledgement

This research was carried out under the project number MC7.07299 in the framework of the Research Program of the Materials Innovation Institute (M2i) (www.m2i.nl). The authors would like to thank Ferdie van Assche from the Holst Centre, the Netherlands, for the preparation of the ITO-SiN_x-PEN sample. Willem-Pier Vellinga and Laurens-Jan. Soer from Groningen University are thanked for making available an independent numerical analysis of the bending shape problem.

References

[1] L. Martinu, D. Poitras, Plasma deposition of optical films and coatings: a review, J. Vac. Sci. Technol. A 18 (6) (2000) 2619–2645.
[2] G.P. Crawford, Flexible Flat Panel Displays, John Wiley & Sons, 2005.
[3] M. Pagliaro, R. Ciriminna, G. Palmisano, Flexible solar cells, ChemSusChem 1 (11) (2008) 880–891.
[4] Y. Leterrier, A. Mottet, N. Bouquet, D. Gilliéron, P. Dumont, A. Pinyol, L. Lalande, J.H. Waller, J.-A.E. Månson, Mechanical integrity of thin inorganic coatings on polymer substrates under quasi-static, thermal and fatigue loadings, Thin Solid Films 519 (5) (2010) 1729–1737.
[5] S. Tarasovs, J. Andersons, Y. Leterrier, Estimation of interfacial fracture toughness based on progressive edge delamination of a thin transparent coating on a polymer substrate, Acta Mater. 58 (8) (2010) 2948–2956.
[6] G.-H. Lee, J. Yun, S. Lee, Y. Jeong, J.-H. Jung, S.-H. Cho, Investigation of brittle failure in transparent conductive oxide and permeation barrier oxide multilayers on flexible polymers, Thin Solid Films 518 (11) (2010) 3075–3080.
[7] A. Pinyol, B. Meylan, D. Gilliéron, V. Mewani, Y. Leterrier, J.-A.E. Månson, Electro-fragmentation analysis of dielectric thin films on flexible polymer substrates, Thin Solid Films 517 (6) (2009) 2000–2006.
[8] S. Grego, J. Lewis, E. Vick, D. Temple, A method to evaluate mechanical performance of thin transparent films for flexible displays, Thin Solid Films 515 (11) (2007) 4745–4752.
[9] Y. Leterrier, L. Médico, F. Demarco, J.-A.E. Månson, U. Betz, M.F. Escolá, N. Kharrazi Olsson, F. Atamny, Mechanical integrity of transparent conductive oxide films for flexible polymer-based displays, Thin Solid Films 460 (1–2) (2004) 156–166.
[10] Y. Leterrier, Durability of nanosized oxygen-barrier coatings on polymers - internal stresses, Prog. Mater. Sci. 48 (1) (2003) 1–55.
[11] G. Rochat, Y. Leterrier, P. Fayet, J.-A.E. Månson, Mechanical analysis of ultrathin oxide coatings on polymer substrates in-situ in a scanning electron microscope, Thin Solid Films 437 (1–2) (2003) 204–210.
[12] D.R. Cairns, R.P. Witte, D.K. Sparacin, S.M. Sachsman, D.C. Paine, G.P. Crawford, R.R. Newton, Strain-dependent electrical resistance of tin-doped indium oxide on polymer substrates, Appl. Phys. Lett. 76 (11) (2000) 1425–1427.
[13] Z. Suo, E.Y. Ma, H. Gleskova, S. Wagner, Mechanics of rollable and foldable film-on-foil electronics, Appl. Phys. Lett. 74 (8) (1999) 1177–1179.
[14] W.P. Vellinga, J.T.M. de Hosson, P.C.P. Bouten, Direct measurement of intrinsic critical strain and internal strain in barrier films, J. Appl. Phys. 110 (4) (2011) 7.
[15] A.A. Abdallah, P.C.P. Bouten, J.M.J. den Toonder, G. de With, Buckle initiation and delamination of patterned ITO layers on a polymer substrate, Surf. Coat. Technol. 205 (2011) 3103–3111.
[16] Q. Guan, J. Laven, P.C.P. Bouten, G. de With, Subcritical crack growth in SiN_x thin-film barriers studied by electro-mechanical two-point bending, J. Appl. Phys. 113 (21) (2013) 213512.
[17] T.Y. Tsui, Y.-C. Joo, A new technique to measure through film thickness fracture toughness, Thin Solid Films 401 (1–2) (2001) 203–210.
[18] S. Zhang, D. Sun, Y. Fu, H. Du, Toughness measurement of thin films: a critical review, Surf. Coat. Technol. 198 (1–3) (2005) 74–84.
[19] M.J. Cordill, Flexible film systems: current understanding and future prospects, J. Mater. 62 (6) (2010) 9–14.
[20] N. Tamura, A.A. MacDowell, R. Spolenak, B.C. Valek, J.C. Bravman, W.L. Brown, R.S. Celestre, H.A. Padmore, B.W. Batterman, J.R. Patel, Scanning X-ray microdiffraction with submicrometer white beam for strain/stress and orientation mapping in thin films, J. Synchrotron Radiat. 10 (2) (2003) 137–143.
[21] C.-H. Ma, J.-H. Huang, H. Chen, Residual stress measurement in textured thin film by grazing-incidence X-ray diffraction, Thin Solid Films 418 (2) (2002) 73–78.
[22] K.J. Martinschitz, R. Daniel, C. Mitterer, J. Keckes, Stress evolution in CrN/Cr coating systems during thermal straining, Thin Solid Films 516 (8) (2008) 1972–1976.
[23] E. Eiper, J. Keckes, K.J. Martinschitz, I. Zizak, M. Cabié, G. Dehm, Size-independent stresses in Al thin films thermally strained down to −100 °C, Acta Mater. 55 (6) (2007) 1941–1946.
[24] P.A. Gruber, J. Böhm, F. Onuseit, A. Wanner, R. Spolenak, E. Arzt, Size effects on yield strength and strain hardening for ultra-thin Cu films with and without passivation: a study by synchrotron and bulge test techniques, Acta Mater. 56 (10) (2008) 2318–2335.
[25] S. Frank, U.A. Handge, S. Olliges, R. Spolenak, The relationship between thin film fragmentation and buckle formation: synchrotron-based in situ studies and two-dimensional stress analysis, Acta Mater. 57 (5) (2009) 1442–1453.
[26] S. Djaziri, D. Faurie, P.-O. Renault, E. Le Bourhis, P.H. Goudeau, G. Geandier, D. Thiaudière, Yield surface of polycrystalline thin films as revealed by non-equibiaxial loadings at small deformation, Acta Mater. 61 (13) (2013) 5067–5077.
[27] A.A. Taylor, V. Edlmayr, M.J. Cordill, G. Dehm, The effect of temperature and strain rate on the periodic cracking of amorphous AlxOy films on Cu, Surf. Coat. Technol. 206 (7) (2011) 1855–1859 (Proceedings of the 38th International Conference on Metallurgical Coatings and Thin Films (ICMCTF) 2011).
[28] A.A. Taylor, V. Edlmayr, M.J. Cordil, G. Dehm, The effect of film thickness variations in periodic cracking: analysis and experiments, Surf. Coat. Technol. 206 (7) (2011) 1830–1836 (Proceedings of the 38th International Conference on Metallurgical Coatings and Thin Films (ICMCTF) 2011).

[29] A. Favache, L. Libralesso, P.J. Jacques, J.-P. Raskin, C. Bailly, B. Nysten, T. Pardoen, Fracture toughness measurement of ultra-thin hard films deposited on a polymer interlayer, Thin Solid Films 550 (0) (2014) 464–471.
[30] H. Jin, W.-Y. Lu, M.J. Cordill, K. Schmidegg, In situ study of cracking and buckling of chromium films on PET substrates, Exp. Mech. 51 (2) (2011) 219–227.
[31] M.J. Cordill, V.M. Marx, Fragmentation testing for ductile thin films on polymer substrates, Philos. Mag. Lett. 93 (11) (2013) 618–624.
[32] A.A. Abdallah, D. Kozodaev, P.C.P. Bouten, J.M.J. den Toonder, U.S. Schubert, G. de With, Buckle morphology of compressed inorganic thin layers on a polymer substrate, Thin Solid Films 503 (24) (2006) 167–176.
[33] P.W. France, M.J. Paradine, M.H. Reeve, G.R. Newns, Liquid nitrogen strengths of coated optical glass fibres, J. Mater. Sci. 15 (1980) 825–830.
[34] M.J. Matthewson, C.R. Kurkjian, S.T. Gulati, Strength measurement of optical fibers by bending, J. Am. Ceram. Soc. 69 (11) (1986) 815–821.
[35] S. Djaziri, P.-O. Renault, F. Hild, E. Le Bourhis, P.H.P. Goudeau, D. Thiaudiere, D. Faurie, Combined synchrotron X-ray and image-correlation analyses of biaxially deformed W/Cu nanocomposite thin films on Kapton, J. Appl. Crystallogr. 44 (5) (2011) 1071–1079.
[36] Q. Guan, Mechanical Reliability of Thin-Film Barriers in Flexible Multilayers, Eindhoven University of Technology, 2015 (PhD thesis);
Q. Guan, J. Laven, P.C.P. Bouten, G. de With, Crack Channeling in Thin-Film Permeation-Barriers Studied by two-Point Rotation Bending and Optical Microscopy (in preparation) 2016.
[37] L.J.M.G. Dortmans, G. de With, Noise sensitivity of fit procedures for Weibull parameter extraction, J. Am. Ceram. Soc. 74 (9) (1991) 2293–2294.
[38] J. Laven, Q. Guan, G. de With, The Electrical Resistance of through-the-Thickness Cracks in a Conductive Strip, 2016 (under review).